The Institute of Space and Astronautical Science
Report No. 596, November 1981

Gas-Particle Nozzle Flows and Optimum Nozzle Shape

By

Takao DOI

(20 August, 1981)

Summary: A computational method to solve the gas-particle flows in axisymmetric nozzles is presented for the prediction of the specific impulse of solid propellant motors. In subsonic-transonic region, the particle phase properties are obtained by numerical integration of the characteristic equations along the particle stream lines, and the method of characteristics is then successfully applied to the supersonic region. The effects of the nozzle size, the throat geometry and the propellants on the thrust performance have been investigated in detail. The comparison between the calculation results and the experimental data shows that the specific impulse of practical motors can be well predicted by specifing the effective particle diameter of 1.8 μ. The optimum nozzle shapes have been also investigated assuming parabolic contours, and a useful design chart for solid propellant motor nozzles is presented.

KEYWORDS
gas-particle flows; equilibrium flow; limiting particle stream line; specific impulse; optimum parabolic shape nozzle

NOMENCLATURE

A; relaxation coefficient of momentum transfer
B; relaxation coefficient of heat transfer
Cp; specific heat of particle
Cpg; specific heat at constant pressure of gas
Dp; particle diameter
ds, dn; line elements of particle stream line
ISP; specific impulse
Kp; particle mass fraction
Mp; material density of particle
P; pressure
Pr; Prandtle number
Qp; $\tan^{-1}(Vp/Up)$
R; gas constant
r_p; radius of particle
Rs; throat radius of curvature
T; temperature

U; x-direction gas velocity component
V; y-direction gas velocity component
W; circumferential gas velocity
x; axial coordinate along nozzle axis
y; radial coordinate measured from nozzle axis
X_E; distance between throat and nozzle exit
Yc; distance between axis and burning surface of solid propellant
Y_E; nozzle exit radius
Yt; nozzle throat radius
Zp; velocity of particle
γ; specific heat ratio of gas
θ; inclination of nozzle wall
μ; viscosity
ρ; density
ω; spin angular velocity

Subscript

e; equilibrium property
o; reference state
p; particle property

1. Introduction

Solid propellants with metal additives are widely used for their high burning temperature. The exhaust products of these propellants contain a large quantity of oxidized metal particles. In case the particles are quite small to have the same velocity and temperature as in the gas phase, the mixture flow can be treated as isentropic flow with modified gas specific heat ratio. Such a flow is named as an equilibrium gas-particle mixture (EGPM). On the contrary, the actual flow is non-equilibrium gas-particle mixture (N-EGPM), and the significant loss in the nozzle thrust performance occurs due to the non-eqlilibrium effects associated with particle drag and heat transfer.

Early investigations [*1* ~ *4*] on the one-dimensional gas-particle nozzle flows showed that the loss in thrust is mainly attributed to the velocity lags between gas and particle phases, and that the non-equilibrium effects become important when the particle diameter is greater than 1 μ.

One of main characteristics of gas-particle nozzle flows is that the mixed flow field is bounded by pure gas flow field generated in the vicinity of the nozzle wall. The boundary originates at the throat inlet section and is called a limiting particle stream line. To treat this complex flow field, it is essential to introduce the two-dimensional profile. Kliegel and Nickerson [*5*] developed the method of characteristics for numerical analyses of gas-particle mixture in axisymmetric nozzles. They also employed Sauer's transonic solution [*6*] and a constant fractional lag assumption to obtain the initial conditions for begining their computation. By using this

method, Kliegel [7], and, Hoffman and Lorenc [8] investigated the characteristic behaviors of gas-particle flows in conical nozzles. Optimum nozzle shapes were also examined by Hoffman and Thompson [9] using the optimum technique made by Guderley and Hantsch [10].

The constant lag assumption, however, is not valid for practical solid propellant motor nozzles. While Regan and et al. [11] used the iterative relaxation technique to solve the transonic flow region, it suffers from some weakness; the assumption of fixed gas phase stream line coordinates, and this procedure is too complicated to be used to practical nozzle designs.

In the present paper, gas-particle nozzle flows are solved by using the method of characteristics and improved calculation procedure of transonic flow field which does not need to assume the constant fractional lag. Transonic solution developed by Oswatitsch and Rothstein [12] is introduced and then the entire nozzle flow field from subsonic-transonic to supersonic region can be solved in series.

Computational results of static pressure, temperature and Mach number distribution in the gas-particle flow field are presented. Variational behaviors of limiting particle stream line due to the motor body spin are also discussed.

The effects of nozzle shape on the thrust performance are investigated in detail varying the size, the throat geometry and the propellants. The calculated thrust performance of actual motors are compared with the experimental data to demonstrate the applicability of present computational method.

Optimum nozzle shapes are investigated to obtain the maximum specific impulse by assuming parabolic nozzle contours and a useful design chart is presented for practical uses.

2. Gas-Particle Flow Model

The conservation equations governing the steady axisymmetric flow of the gas-particle mixture are derived under the following assumptions:

(1) The total mass and total energy of the system remain constant.
(2) The gas is perfect gas and inviscid except for its interactions with the particles.
(3) The heat capacity of the gas and particles is constant.
(4) The gas and particles do not undergo phase changes.
(5) The internal temperature of the particles is uniform.
(6) The thermal (Brownian) motion of the particles is negligible.
(7) The volume occupied by the particles is negligible.
(8) The particles do not interact each other.
(9) The characteristics of an actual shape and size distribution of particles can be represented by spherical particles of a single size.
(10) Energy exchange between gas and particles occurs only by convection.
(11) The only force on the particles is viscous drag force which is subject to Stokes' drag law.

Using these assumptions, the equations governing the gas-particle flows are given

as follows:

Gas Phase

continuity equation

$$\frac{\partial \rho Uy}{\partial x} + \frac{\partial \rho Vy}{\partial y} = 0 \tag{1}$$

axial and radial momentum equations

$$\rho U \frac{\partial U}{\partial x} + \rho V \frac{\partial U}{\partial y} + \frac{\partial P}{\partial x} + A\rho_p(U-Up) = 0 \tag{2}$$

$$\rho U \frac{\partial V}{\partial x} + \rho V \frac{\partial V}{\partial y} + \frac{\partial P}{\partial y} + A\rho_p(V-Vp) = 0 \tag{3}$$

energy equation

$$U\frac{\partial P}{\partial x} + V\frac{\partial P}{\partial y} - \gamma RT\left(U\frac{\partial \rho}{\partial x} + V\frac{\partial \rho}{\partial y}\right) - (\gamma-1)\rho_p\{A(U-Up)^2 + A(V-Vp)^2 - BCp(T-Tp)\} = 0 \tag{4}$$

equation of state

$$P = \rho RT \tag{5}$$

Particle Phase

continuity equation

$$\frac{\partial \rho_p Upy}{\partial x} + \frac{\partial \rho_p Vpy}{\partial y} = 0 \tag{6}$$

axial and radial momentum equations

$$\rho_p Up \frac{\partial Up}{\partial x} + \rho_p Vp \frac{\partial Up}{\partial y} - A\rho_p(U-Up) = 0 \tag{7}$$

$$\rho_p Up \frac{\partial Vp}{\partial x} + \rho_p Vp \frac{\partial Vp}{\partial y} - A\rho_p(V-Vp) = 0 \tag{8}$$

energy equation

$$\rho_p Up \frac{\partial Tp}{\partial x} + \rho_p Vp \frac{\partial Tp}{\partial y} - B\rho_p(T-Tp) = 0 \tag{9}$$

where

$$A = \frac{9\mu}{2Mpr_p^2} \cdot \frac{Yt}{U_0} \tag{10}$$

$$B = \frac{3\mu}{PrMpr_p^2} \cdot \frac{Cpg}{Cp} \cdot \frac{Yt}{U_0} \tag{11}$$

suffix p denotes the values of the particle phase. A and B are relaxation coefficients of momentum and heat transfer, respectively. Pr is Prandtle number, which is computed using Euken's relation as follows:

$$Pr=\frac{4\gamma}{9\gamma-5} \tag{12}$$

Cpg is the specific heat of constant pressure of the gas phase. Mp is the material density of the particles, and r_p is an effective radius of particles. μ is the viscosity of the gas phase and computed using Southerland's formula,

$$\mu=\mu_0\left(\frac{T+c}{T_0+c}\right)\left(\frac{T}{T_0}\right)^{3/2} \tag{13}$$

where μ_0 is the reference viscosity at $T=T_0$, and c is the material constant.

3. Computational Model

The flow field of the gas-particle mixture is divided into two computational regions. The solution of the subsonic-transonic region gives the initial condition to carry on the supersonic flow calculation.

In the first region, we assume that gas phase properties can be treated as those of EGPM with the following specific heat ratio,

$$\gamma e=\frac{(1-Kp)Cpg+KpCp}{(1-Kp)(Cpg-R)+KpCp} \tag{14}$$

where Kp is the particle mass fraction to the total mixture mass. This assumption is correct in the case of small particles. Transonic solution developed by Oswatitsch and Rothstein [*12*] is applied to obtain the properties of EGPM. To solve the particle phase behavior, the governing equations ($6\sim9$) are rewritten along a particle stream line as follows:

$$\text{along}\ \frac{dy}{dx}=\frac{Vp}{Up}$$

$$UpdUp-A(U-Up)dx=0 \tag{15}$$

$$VpdVp-A(V-Vp)dy=0 \tag{16}$$

$$UpdTp-B(T-Tp)dx=0 \tag{17}$$

$$d(\rho_pZp)+\left(\rho_pZp\frac{dQp}{dn}+\frac{\rho_pVp}{y}\right)ds=0 \tag{18}$$

where

$$Zp=\sqrt{Up^2+Vp^2} \tag{19}$$

$$Qp=\tan^{-1}\frac{Vp}{Up} \tag{20}$$

ds and dn are line elements in tangential and normal directions of a particle stream line, respectively.

Above equations are characteristic equations in the particle phase and computed along each particle stream line using the gas phase flow field, $U(x, y)$, $V(x, y)$, and $T(x, y)$, as the driving functions. The limiting particle stream line is a trajectory of the nearest particle to the nozzle wall. The modified Euler's method is used to calculate the values in each point. In this method, it is necessary to satisfy the following computational convergence conditions [*13*]:

$$\frac{1}{2}A\Delta H<1 \tag{21}$$

$$\frac{1}{2}B\Delta H<1 \tag{22}$$

where ΔH is the distance between two neighboring points. Since it is needless to assume the constant fractional lag in this transonic flow calculation, we can evaluate the effects of gas properties on particle properties more exactly.

The numerical method of characteristics is then applied to solve the supersonic flow field of the gas-particle mixture. The characteristic equations of the gas phase are derived as follows:

$$\text{along}\ \frac{dy}{dx}=\frac{V}{U}$$

$$\rho UdU+\rho VdV+dP+A\rho_p(U-Up)dx+A\rho_p(V-Vp)dy=0 \tag{23}$$

$$UdP-\gamma RTUd\rho-(\gamma-1)\rho_p\{A(U-Up)^2+A(V-Vp)^2-BCp(T-Tp)\}dx=0 \tag{24}$$

$$\text{along}\ \frac{dy}{dx}=\frac{UV\pm\sqrt{\gamma RT(U^2+V^2)-\gamma RT}}{U^2-\gamma RT}$$

$$\rho\gamma RT(VdU-UdV)+\left(\gamma RT\frac{dy}{dx}+UV-U^2\frac{dy}{dx}\right)dp-\frac{\rho\gamma RTV}{y}(Udy-Vdx)$$
$$-(\gamma-1)\rho_p\{A(U-Up)^2+A(V-V_p)^2-BCp(T-Tp)\} \tag{25}$$
$$+\gamma RT\rho_pA\{(U-Up)dy-(V-Vp)dx\}=0$$

There are four characteristic equations on three characteristic lines; i.e., gas stream line, left running and right running characteristic lines. In total system including the particle phase, there are eight characteristic equations on four characteristic lines. This characteristic system is completely the same as the fundamental system described by the equations ($1\sim9$). The number of initial data line points which are obtained by the subsonic-transonic flow calculation determines the mesh size throughout the nozzle flow field. The modified Euler's method is also used to

calculate the values in each characteristic point.

4. Characteristics of Gas-Particle Nozzle Flows

4–1. Typical flow field

In this section, we discuss the characteristics of the gas-particle flow field in a conical nozzle whose data is shown in Table 1.

Fig. 1 and Fig. 2 illustrate the lines of constant Mach number of EGPM and

Table 1. Conical nozzle configuration

Nozzle inlet angle:	30°
Conical angle:	25°
Throat radius:	0.075 m
Throat radius of curvature:	0.3 m
Nozzle length:	0.75 m
Nozzle exit radius:	0.394 m

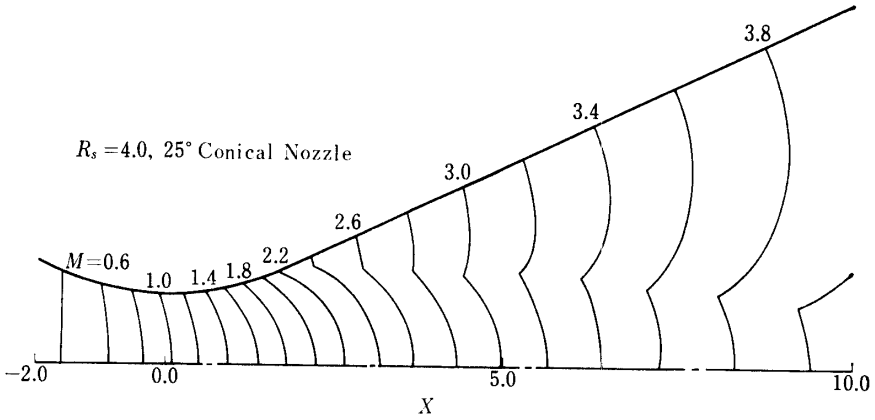

Fig. 1. Line of constant Mach number in equilibrium flow.

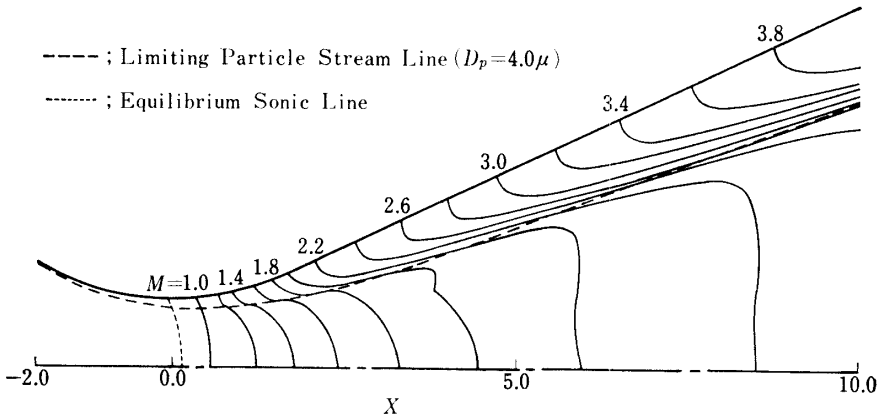

Fig. 2. Line of constant Mach number in non-equilibrium flow.

N-EGPM, respectively. The gas properties are specified as $\gamma = 1.293$, molecular weight (Mw) = 18.2, chamber temperature (To) = 3189°K, chamber pressure (Po) = 51.66 kgw/cm^2. Aluminum oxide particles of 4μ in diameter are assumed, and its mass flow rate (Kp) is taken as 30% of the total mass flow rate. The number of initial points for calculation is chosen as 50.

Fig. 1 shows the entire flow field in equilibrium flow with modified gas specific heat ratio (γe) of 1.2. The existence of cusps on the lines of constant Mach number in supersonic region is caused by the different expansion characteristics induced by the circular arc and straight nozzle wall. These points are on the right running characteristic line departing from the joint of the both walls.

The lines of constnat Mach number of non-equilibrium flow shown in Fig. 2 greatly change due to the existence of particle of 4μ. A thin dashed line denotes a sonic line of equilibrium flow, and a thick dashed line stands for a limiting particle stream line. In the region between the nozzle wall and this line, only the pure gas phase exists. All particles of a given size are located between the axis and this limiting particle stream line. It is seen that the cusps on the lines of constant Mach number are not remarkable in contrast to the case of EGPM. It is also seen that there is a layer of finite thickness along the limiting particle stream line where a strong velocity gradient exists. The layer is caused by the assumption of single particle size for the calculation. As there must be a particle size distribution in an actual flow, the velocity difference in this layer is not supposed to be so large.

Fig. 3 shows the pressure distribution along both the nozzle axis and the wall. Pressure value is non-dimensionalized by the chamber pressure. It is seen that the

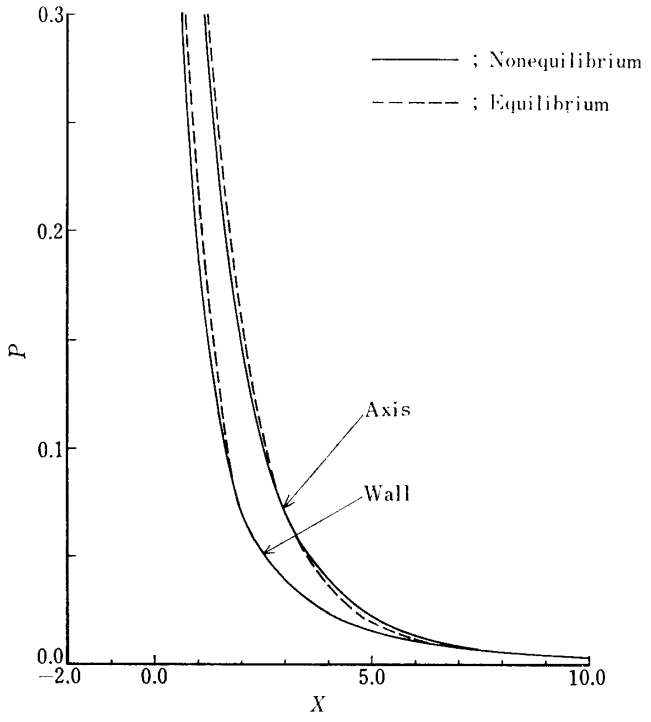

FIG. 3. Pressure distribution.

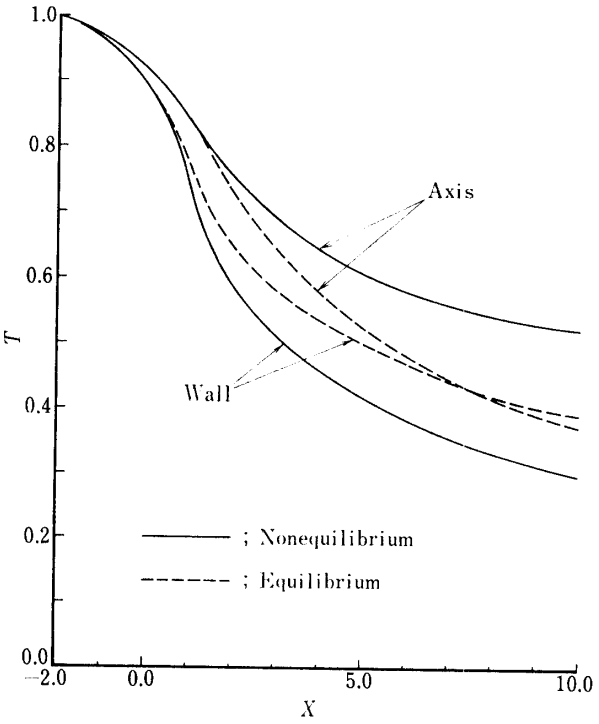

FIG. 4. Temperature distribution in gas phase.

pressure of EGPM is higher than that of N-EGPM in the initial expansion region. This difference directly indicates the thrust loss since the thrust produced by the nozzle is obtained by integrating the static pressure along the nozzle wall. The existence of particle phase prevent the gas phase expansion, and it is caused by this phenomenon that the pressure of N-EGPM is higher than that of EGPM along the axis from $x=3.0$ to $x=7.0$.

Fig. 4 shows the gas phase temperature distribution along both the nozzle axis and the wall. Temperature value is non-dimensionalized by the chamber temperature. It is seen that the temperature of N-EGPM along the axis is higher than that of EGPM. Because of the high concentration of the hot particles to the nozzle axis, the gas phase near the nozzle axis is heated locally by the particle phase.

Fig. 5 is a plot of the axial velocity lag for various sizes of particles on the limiting particle stream line. It is seen that the particle fractional lag is almost constant near the throat region, and good agreement between present method and Kliegel's constant fractional lag approximation method is obtained when the particle diameter is less than 2μ. When the particle diameter is larger than 2μ, Kliegel's method indicates the larger values in comparison with the present method. Dominant effect of the particle size on the particle velocity lag is seen clearly. The maximum velocity lag is observed at the throat section, therefore it should be noted that the thrust performance loss associated with the non-equilibrium effects mainly occur at the throat section.

Fig. 6 is a plot of the thermal lag on the limiting particle stream line for various size of particle. The points indicated by arrows are located at the intersection of limiting particle stream line and the right running characteristic line departing from

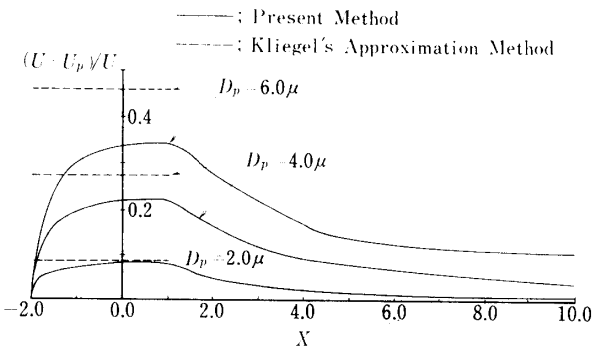

FIG. 5. Particle velocity lag of axial direction on limiting particle stream line.

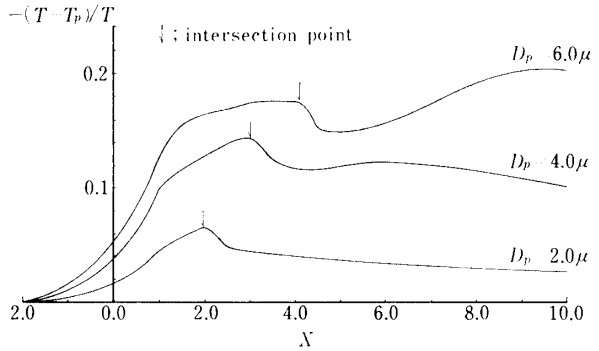

FIG. 6. Particle temperature lag on limiting particle stream line.

the joint of circular arc wall and streight nozzle wall. The particle size is seen to have also a great effect on the particle thermal lag.

4–2. Spin Effect on Limiting Particle Stream Line

The spin stabilization is widely used for sounding rockets and solid upper stages. The spin rate is not so high, and ordinarily it is 2 or 3 rps. Here we consider these spin effects on the gas-particle nozzle flow field. It is assumed that the flow field rotates around the nozzle axis keeping constant angular momentum along each stream line. This assumption is correct when the circumferential velocity is small in comparison with the axial velocity, since the gas phase and the particle phase have almost the same circumferential velocities. Based on this assumption, the momentum equations of the radial direction are given as follows:

$$\rho U\frac{\partial V}{dx}+\rho V\frac{\partial V}{\partial y}+\frac{\partial P}{\partial y}+A\rho_p(V-Vp)-\frac{\rho W^2}{y}=0 \tag{26}$$

$$\rho_p Up\frac{\partial Vp}{\partial x}+\rho_p Vp\frac{\partial Vp}{\partial y}-A\rho_p(V-Vp)-\frac{\rho_p Wp^2}{y}=0 \tag{27}$$

where [*14*]

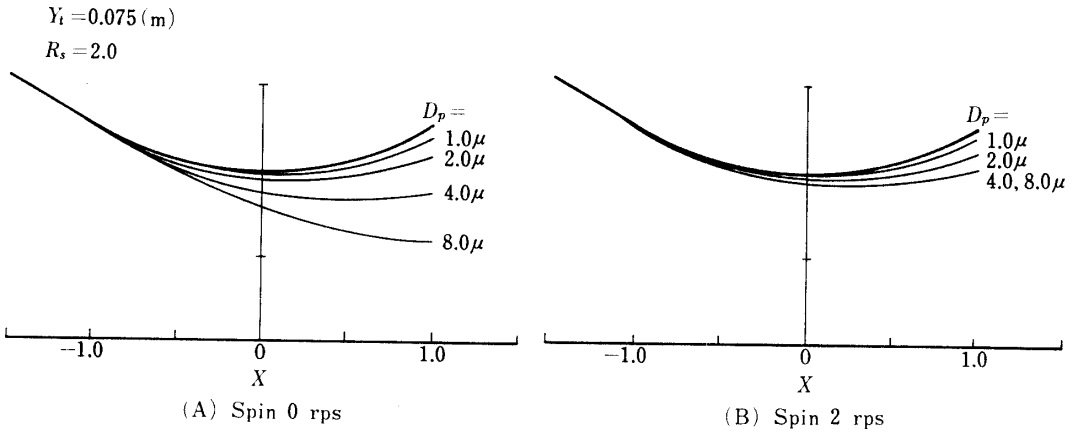

FIG. 7. Spin effect on limiting particle stream line.

$$W = Wp = \frac{\omega Yc^2}{y} \tag{28}$$

W and Wp are the circumferential velocities of the gas and the particle phases, respectively. ω is the spin angular velocity, and Yc is the radial distance between the spin axis and the burning surface of solid propellant.

The last terms of left hand side of both equations denote the centrifugal forces. These forces are ordinarily very small comparing with the other terms. Therefore this term is negligible in the gas phase. In the particle phase, however, it comes a significant term near the throat region where the viscous term becomes negligible. By this reason, the location of the particle stream line near the throat region is very affected by the motor body spin.

Fig. 7 shows the effects of the motor body spin on the limiting particle stream line near the throat region for various particle sizes. The calculations are performed about the circular arc throat section with throat radius of 0.075 m, throat radius of curvature of 0.15 m, inlet angle of 30°. Yc is specified to 1.5 m. The spin rate is assumed 2 rps. It is seen that the location of the limiting particle stream line of the particles whose diameters are greater than 4μ is changed dramatically. These changes of the limiting particle stream lines increase the possibility of the particle impingement with the normally-designed nozzle walls ignoring the spin effect. Therefore, when we design the nozzle contour of the motor for spinstabilized stage, we need countermeasures to avoid the particle impingement.

5. CHARACTERISTICS OF NOZZLE PERFORMANCE

5–1. Design Parameters of Nozzle Shape

The fundamental nozzle design parameters are shown in Fig. 8. These parameters are as follows:

(1) Yt; Throat Radius

(2) X_E; Nozzle Length (Distance between throat and exit plain)

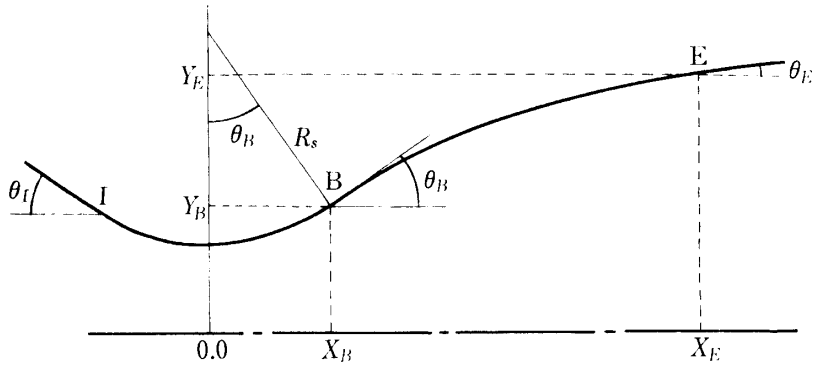

FIG. 8. Design parameter.

(3) Y_E; Nozzle Exit Radius
(4) Rs; Throat Radius of Curvature
(5) θ_I; Nozzle Inlet Angle
(6) θ_B; Initial Expansion Angle
(7) θ_E; Exit Divergence Angle

A nozzle configuration is selected with a conical inlet section whose slope angle is θ_I and a circular arc throat section whose redius is Rs. Rs, X_E and Y_E are non-dimensionalized by the throat radius. In addition to these parameters, various nozzle contours can be adequately chosen, for example, circular arcs, parabolic arcs, hyperbolic arcs, and etc. The parabolic arcs specially have been reported by Rao [*15*] to be a close approximation to the exact optimum nozzle contour. Therefore in the following discussion, we adopt the parabolic arc as the nozzle contour.

5–2. *Scale Effect*

In the gas-particle flow system, it is need to satisfy the following condition to obtain the similar flow field,

$$\frac{Yt}{r_p^2} = \text{const.} \tag{29}$$

This relation is one of main characteristics of the gas-particle non-equilibrium mixture, which is not seen in the case of equilibrium flow.

Fig. 9 shows the scale change effect on the thrust performance of the conical nozzles which have the similar configuration with inlet angle of 30°, cone angle of 25°, throat radius of curvature of 2.0, nozzle length of 10.0 and nozzle exit radius of 5.46. The propellant is BP-30B. The divergence loss which is caused by the two-dimensional effect is constant, but the two-phase flow loss is observed to be sensitive to the change of the throat radius and to be severe in the small size motors. The particle diameter also has great effect on the thrust performance.

Fig. 10 illustrates the scale effect on the limiting particle stream line of 2μ diameter particle. Smaller the motor size is, nearer the location is to the nozzle axis. It is seen, however, that the actual distance between the limiting particle stream line and the wall is almost the same in each case.

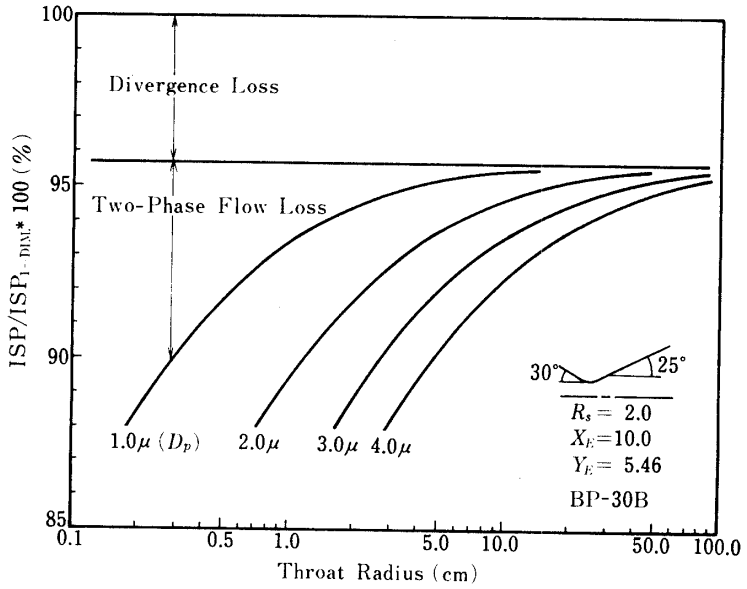

FIG. 9. Scale effect on thrust performance.

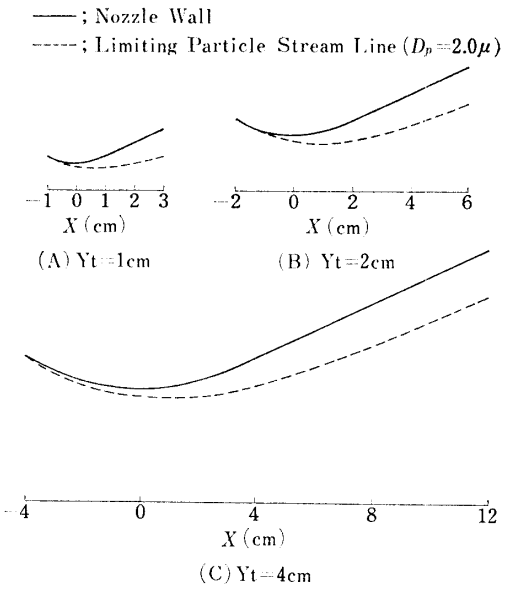

FIG. 10. Scale effect on limiting particle stream line.

Fig. 11 shows the scale effect on Specific impulse varying the solid propellants whose data is presented in Table 2. A nozzle configuration is selected to be a bell type with inlet angle of 30°, initial divergence angle of 32°, throat radius of curvature of 2.0, nozzle length of 10.0, and nozzle exit radius of 4.92.

Ordinarily, the performance of solid propellants has been estimated by EGPM evaluation which are indicated by dashed lines on the figure, and it gives valid results in the case of relatively large size motors. However, it can be observed that the EGPM evaluation is not suitable in the case of small size motors. For example, the performance of BP-27B is superior to those of BP-20B and BP-30B

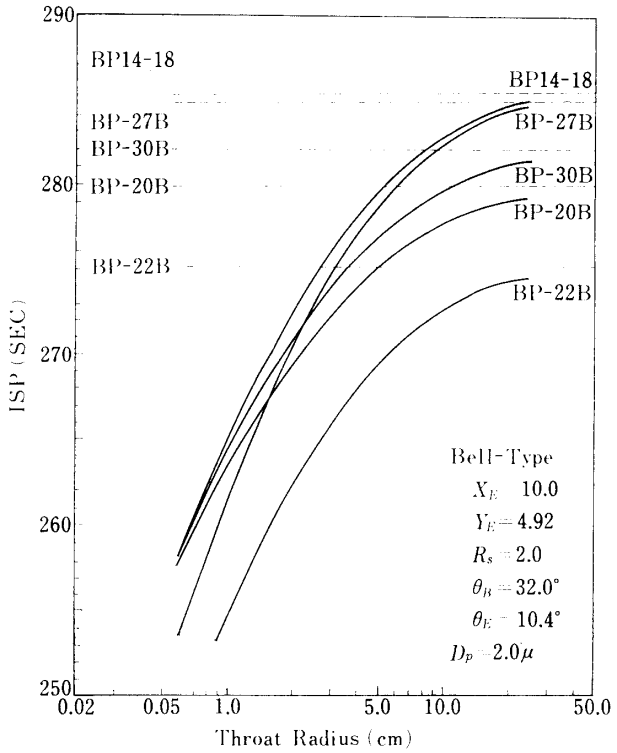

FIG. 11. Scale effect on ISP of various propellants.

TABLE 2. Propellant data

Name	BP-20B	BP-22B	BP-27B	BP-30B	BP14-18
Composition (mass fraction)					
AP	0.67	0.64	0.66	0.68	0.68
CTPB	0.17	0.18	0.14	0.16	0.14
Al	0.16	0.18	0.20	0.16	0.18
Mean molecular mass	25.49	25.15	27.90	26.09	27.613
Flame temperature (°K)	3049	2928	3367	3144	3349
Equiliburium specific heat ratio (γe)	1.2078	1.2122	1.1922	1.2035	1.1936
Particle mass fraction (K_D)	0.302	0.34	0.378	0.302	0.34

according to the EGPM evaluation. On the contrary, BP-20B and BP-30B have higher ISP-performance than BP-27B when the throat radius is less than 2.0 cm and 1.5 cm, respectively. This result is due to the high particle mass fraction of BP-27B. It is noted that this tendency will be clearer when the particle mass fraction is higher and the particle diameter is larger. BP14–18 can be seen to have the best ISP-performance in almost all ranges of throat radius.

5–3. Throat Curvature Effect

In order to estimate the effect of throat wall shape on the thrust performance, calculations are performed with varying the throat radius of curvature (Rs). A

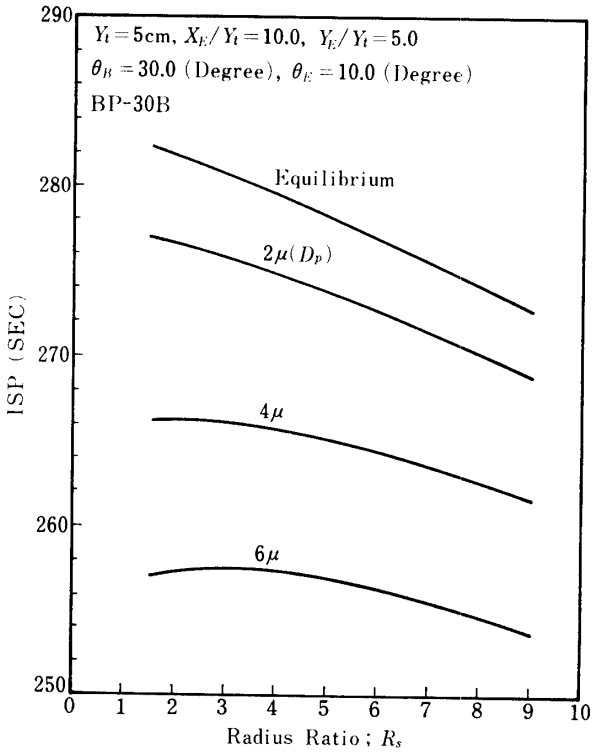

FIG. 12. Rs effect on thrust performance.

TABLE 3. ISP Efficiency (ISP_{N-EGPM}/ISP_{EGPM})

Rs	2.0	4.0	6.0	8.0
EGPM	1.0	1.0	1.0	1.0
2 μ	0.981	0.983	0.985	0.986
4 μ	0.943	0.951	0.955	0.958
6 μ	0.913	0.921	0.926	0.930

nozzle configuration is selected with inlet angle of 30°, initial expansion angle of 30°, exit divergence angle of 10°, nozzle length of 10, and nozzle exit radius of 5. The propellant is BP-30B. The results are shown in Fig. 12.

The case of EGPM gives the maximum theoretical delivered specific impulse, and it gradually decreases when *Rs* increases. In the case of 4μ and 6μ diameter particles, however, it is seen that the optimum *Rs*-values exist which produce the maximum specific impulse. For example, the optimum *Rs* is about 2.0 and 3.0 in the case of 4μ and 6μ particles, respectively.

ISP efficiencies of various particle sizes are presented in Table 3. It is observed that there is slight increase in ISP efficiency as the radius of curvature is increased. This trend is attributed to the lower particle lag since the acceleration rate in the throat section decreases with increasing the throat radius of curvature, and it comes clearer with increasing the particle diameter.

Fig. 13 shows the *Rs*-effect on the location of the limiting particle stream line of 4μ diameter particle. It is seen that its location becomes nearer to the nozzle

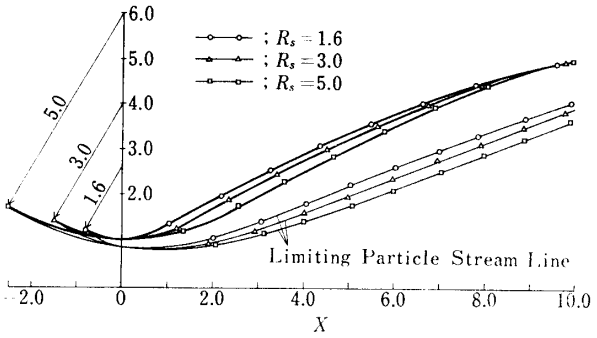

FIG. 13. Rs-Effect on limiting particle stream line.

wall with decreasing the throat radius of curvature. The differences of their location are mainly induced by the nozzle wall shape at the initial expansion region.

5-4. Comparison of Measured and Calculated Thrust Performance

Particle diameter is one of the major factors to be specified to evaluate the practical motor performance. For this purpose, the comparison of measured and calculated ISP is performed, and results are shown in Fig. 14. The experimental data is presented in Table 4. These small motors are for upper stages, and the experiments were performed in vacuum chambers.

Solid lines on the figure denote the calculation values, which are very sensitive to the particle diameter. Inclination of these lines is concerned with the throat radius, i.e., the scale effect as previously mentioned in section 5-2. It is shown that smaller the nozzle size is, larger the inclination is. Circular markes on these lines denote the experimental values.

It is found that the calculated thrust performance is in good agreement with the experimental data when the particle diameter is specified to 1.8μ. This particle diameter should be considered to be an effective diameter, since present calculations do not include the effects of heat loss and nozzle friction. It is noted that this diameter is almost the same as the size of the particles gathered in the experiment [*13*].

According to the recent investigations [*16* ~ *19*], the particle size is a function of throat radius and chamber pressure. Therefore, the careful further investigations will be needed to predict the thrust performance of all size motors.

TABLE 4. Experimental data of solid motors

No.	Yt(m)	Rs	X_E	Y_E	Propellant	ISP (sec)
1	0.052	1.92	14.23	6.69	BP-27B	289.5
2	0.0175	2.29	17.94	7.07	BP-27B	283.0
3	0.0540	1.61	13.70	6.44	BP-20B	284.0
4	0.0295	2.10	14.41	6.44	BP-20B	281.4

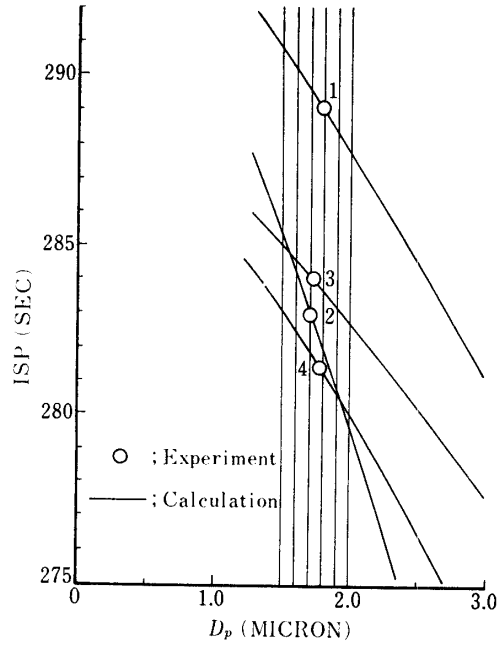

FIG. 14. Comparison of measured and calculated thrust performance.

6. OPTIMUM NOZZLE SHAPE

6–1. Characteristics of Optimum Nozzle Shape

Fig. 15 illustrates the relations among design parameters, X_E, Y_E, and θ_B of the maximum thrust nozzles. The effects of exit divergence angle (θ_E) on the thrust performance is ignored since it can be found to be relatively small in comparison with the effects of the other parameters. The nozzle shapes are optimized with respect to the nozzle length (X_E) by using Fibonacci search method. The following wall function is used as a parabolic contour,

$$Y(X)=a(X-X_B)^2+b(X-X_B)+Y_B \tag{30}$$

where

$$a=\frac{Y_E-Y_B-\mathrm{Tan}\,\theta_B(X_E-X_B)}{(X_E-X_B)^2} \tag{31}$$

$$b=\mathrm{Tan}\,\theta_B \tag{32}$$

The solid line and dashed line on the figure denote the case of N-EGPM and EGPM, respectively.

It is observed that the both cases give the similar results. The exit radius of N-EGPM, however, is slightly smaller than that of EGPM because of decreasing the divergence loss of the particle phase which has relatively straight stream line.

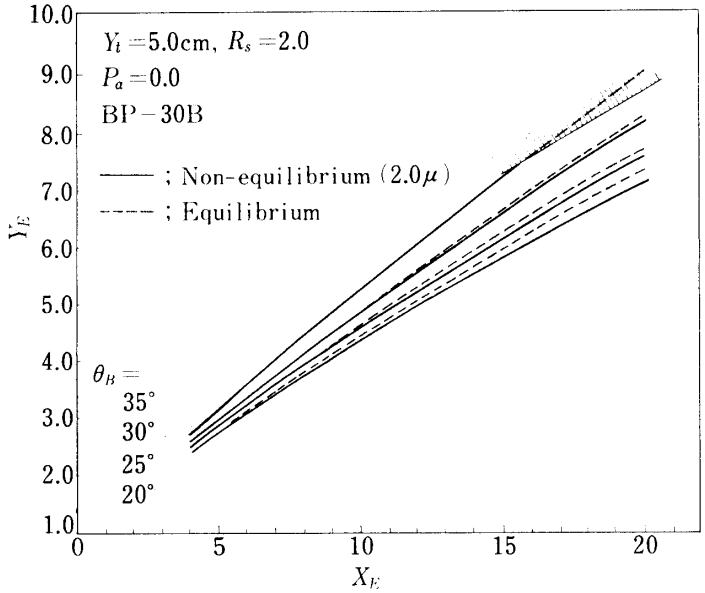

FIG. 15. Characteristics of optimum parabolic shape nozzle.

The difference of the exit radius of both cases decreases as the initial expansion angle increases. The optimum contours are identical when the initial expansion angle is 35°. It is caused by the difference of particle distribution of radial direction. In the case of large initial expansion angle, the particle density is small as the particles are widely distributed. In other words, the flow characteristics tend to those of equilibrium flow.

The shadowed domain denotes the region where particles impinge on the nozzle wall. These impingements cause a significant thrust loss and nozzle wall damage [*20*]. Therefore, we should not design the nozzle shape in this domain.

6–2. Optimum Nozzle Design Chart

From the view point of the practical design, it will be convenient to know the relations among the design parameters of the optimum nozzle at a glance. For this purpose, Rao [*15*] made a design chart of optimum nozzle shape, which could not include the data of thrust performance.

A new design chart for the optimum parabolic shape nozzle is presented in Fig. 16. This chart provides the relation among the thrust performance and various design parameters. Using this chart, we can design the optimum nozzle shape easily under the following given parameters:

(1) nozzle length
(2) nozzle exit radius
(3) nozzle length and nozzle exit radius
(4) ISP and nozzle length
(5) ISP and nozzle exit radius

For example, in the first case the design point is the maximum point of a constant nozzle length line, and in the fifth case it is the intersection of a constant thrust line and a constant exit radius line. This chart is for the non-equilibrium flow nozzle

with zero ambient pressure. And it is easy to draw the design charts for various ambient pressure and throat geometry.

To demonstrate the thrust gain of the optimum parabolic shape nozzle, the thrust of the nozzles designed for 2μ diameter particle are compared with those of the

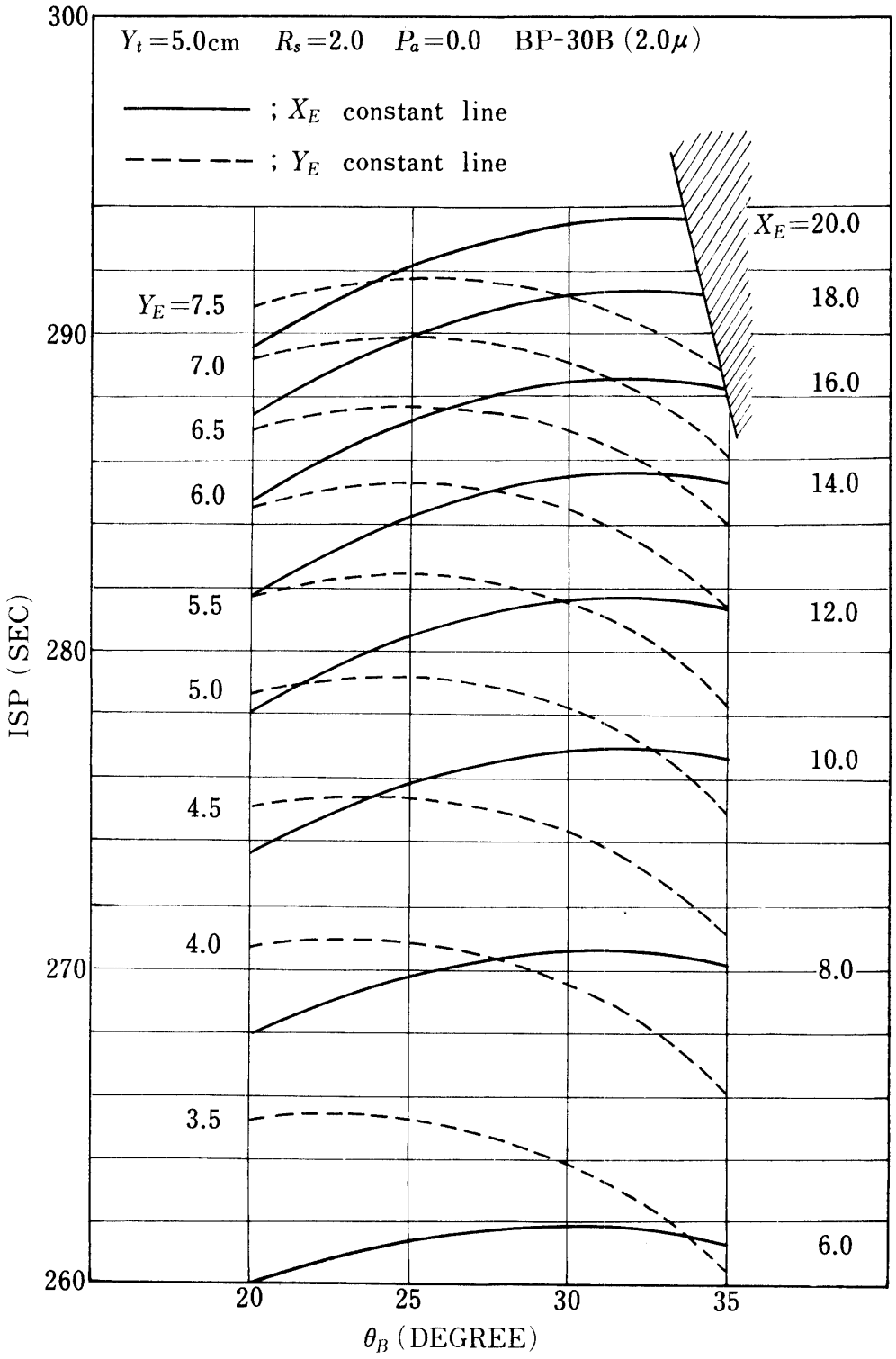

FIG. 16. Design chart for optimum parabolic shape nozzle.

conical nozzles with the same length. The results are presented in Table 5.

The thrust gain of the optimum nozzle relative to the 22°conical nozzle is 1.31%. The 22°conical nozzle is the best in all conical nozzles of various conical angles. The other example is the case of Pa/Po=0.01. Comparing with the 15°conical nozzle, the thrust gain is 0.88%. Those thrust gains are almost the same as those of previous investigations performed by Hoffman and Elsbend [21]. Therefore, the present design method using the parabolic contour is quite useful for solid motor nozzle designs.

TABLE 5. Comparison of thrust performance

	Pa/Po	*Rs*	X_E	Y_E	θ_B	ISP (sec)	GAIN (%)
optimum	0.0	2.0	14.0	6.43	32°	285.6	1.31
22°conical	0.0	2.0	14.0	6.50	22°	281.9	—
optimum	0.01	2.0	8.0	3.11	22°	251.0	0.88
15°conical	0.01	2.0	8.0	3.07	15°	248.8	—

7. CONCLUSION

The entire gas-particle flow fields in axisymmetric nozzles are studied by using the improved transonic flow field calculation and the method of characteristics. It has been shown that there is a layer of finite thickness along the limiting particle stream line where a strong velocity gradient exists, and that the thrust performance losses mainly occur at the throat section. It has been also found that the limiting particle stream line is deflected towards the nozzle wall by the centrifugal force generated by the motor body spin.

Next, the effects of nozzle shape on the thrust performance have been investigated in detail. The results can be summarized as follows:

(1) Thrust loss due to the non-equilibrium effects increases with decreasing the nozzle scale, and it is very severe in the case of small size motors.

(2) ISP efficiency ($ISP_{N\text{-}EGPM}/ISP_{EGPM}$) increases with increasing the throat radius of curvature, *Rs*, and the optimum value of *Rs* exists when the particle diameter is larger than 4μ.

(3) The thrust performance of relatively small size motors are well predicted by the present computational method specifing an effective particle size of 1.8μ.

(4) The exit radius of the optimum parabolic shape nozzle in the case of N-EGPM is slightly smaller than that in the case of EGPM, under the restriction of fixed nozzle length and fixed initial expansion angle.

In addition, it has been shown that N-EGPM evaluation is needed to estimate the exact ISP-performance of the solid propellants, particularly that of propellants which contain large quantity of aluminum particles.

Finally, a useful design chart for the optimum parabolic shape nozzle is presented, and it has been shown that the good thrust gains can be obtained by this procedure.

ACKNOWLEDGEMENT

The author wishes to express his gratitude to Prof. Ryojiro Akiba and Dr. Masahiro Kohno for their useful instructions and advices through this work.

REFERENCES

[1] W. S. Bailey, E. N. Nilson, R. A. Serra and T. F. Zupnik: "Gas-Particle Flow in Axisymmetric Nozzle", ARS J., July 1961, pp. 793–798.
[2] R. D. Glauz: "Combined Subsonic-Supersonic Gas-Particle Flow", ARS J., May 1962, pp. 773–775.
[3] R. F. Hoglund: "Recent Advances in Gas-Particle Nozzle Flows", ARS J., May 1962, pp. 662–671.
[4] F. E. Marble: "Nozzle Contours for Minimum Particle-Lag Loss", AIAA J., Vol. 1, No. 12, December 1963, pp. 2793–2801.
[5] J. R. Kligel and G. R. Nickerson: "Flow of Gas-Particle Mixtures in Axially Symmetric Nozzles", Detonation and Two-Phase Flow (Academic Press, 1962) pp. 173–195.
[6] R. Sauer: "General Characteristics of the Flow Through Nozzles at Near Critical Speeds", NASA, TM., No. 1147.
[7] J. R. Kliegel: "Gas-Particle Nozzle Flows", Ninth Symposium on Combustion (Academic Press, New York, 1963) pp. 811–826.
[8] J. D. Hoffman and S. A. Lorenc: "Parametric Study of Gas-Particle Flows in Conical Nozzle", AIAA J., Vol. 3, No. 7, January 1965, pp. 103–106.
[9] J. D. Hoffman and H. D. Thompson: "A General Method for Determining Optimum Thrust Nozzle Contours for Gas-Particle Flows", AIAA Paper, No. 66–538.
[10] K. G. Guderley and J. V. Armitage: "General Approach to Optimum Rocket Nozzles", Theory of Optimum Aerodynamic Shapes (Academic Press, New York, 1965) pp. 161–183.
[11] J. F. Reagan, H. D. Thompson and R. F. Hoglund: "Two-Dimensional Analysis of Trasonic Gas-Particle Flows in Axisymmetric Nozzles", J. Spacecraft, Vol. 8, No. 4, April 1971, pp. 346–351.
[12] K. L. Oswatitsch and W. Rothstein: "Flow Pattern in a Converging-Diverging Nozzle", NACA, TM., No. 1215.
[13] T. Doi: "Gas-Particle Nozzle Flows and Optimum Nozzle Shape" Master Thesis, University of Tokyo, March 1980 (in Japanese).
[14] A. Marger: "Approximate Solution of Isentropic Swirling Flow through a Nozzle", ARS J., Vol. 31, No. 8, August 1961, pp. 1140–1148.
[15] G. V. Rao: "Approximation of Optimum Thrust Nozzle Contour" ARS J., Vol. 30, No. 6, June 1960, pp. 561.
[16] J. L. Eisel, B. G. Brown and E. W. Price: "Pressure, Velocity and Geometry Effection Al_2O_3 Produced During Aluminized Propellant Combustion", AIAA J., Vol. 13, No. 7, July 1975, pp. 913–917.
[17] "Solid Rocket Motor Performance Analysis and Prediction", NASA, SP-8039, May 1971.
[18] N. S. Cohen, D. P. Harry, C. F. Price, D. E. Coats, J. N. Levine and G. R. Nickerson: "Solid Rocket Performance Prediction Techniques", AIAA Paper, No. 74–1200.
[19] E. M. Landsbaum, M. P. Salinas and J. P. Leary: "Specific Impulse Prediction of Solid-Propellant Motors", J. Spacecraft, Vol. 17, No. 5, Sept.–Oct. 1980, pp. 400–406.
[20] W. L. Daines, T. A. Boardman, R. K. Lund and R. Abel: "Effect of Aluminum Oxide Impingement on Specific Impulse of Solid Propellant Motors", AIAA Paper, No. 75–1277.
[21] J. D. Hoffman and A. A. Elsbernd: "Maximum Thrust Nozzles for Gas-Particle Flows", AIAA J., Vol. 12, No. 3, March 1974, pp. 283–288.